Electromechanical response of micromachined 1-3 piezoelectric composites: Effect of etched piezo-pillar slope

Xiaohua Jian, Sibo Li, Wenbin Huang, Yaoyao Cui and Xiaoning Jiang

Journal of Intelligent Material Systems and Structures published online 20 August 2014
DOI: 10.1177/1045389X14546657

Original Article

Journal of Intelligent Material Systems and Structures

Journal of Intelligent Material Systems and Structures
1–9

DOI: 10.1177/1045389X14546657
jim.sagepub.com
SAGE

Electromechanical response of micromachined 1-3 piezoelectric composites: Effect of etched piezo-pillar slope

Xiaohua Jian[1,2], Sibo Li[1], Wenbin Huang[1], Yaoyao Cui[2] and Xiaoning Jiang[1]

Abstract

Micromachined single-crystal piezoelectric 1-3 composites are known for high electromechanical coupling coefficients, low acoustic impedance, high processing precision and uniformity, which are desired for high-frequency ultrasound transducers. In this article, based on Smith and Auld's 1-3 composite thickness-mode oscillation model, the effect of etched side wall slope on the electromechanical characteristics of micromachined piezoelectric 1-3 composites was studied. In specific, strain constant, stiffness, dielectric constant, electromechanical coupling coefficient, acoustic impedance, longitudinal velocity, and frequency of micromachined 1-3 composites were deduced using the developed model. The analytical model was then verified by a COMSOL simulation and experimental measurements of a micromachined composite sample with pitch of 15.9 μm, thickness of 42.8 μm, and etched pillar slope angle of 83.8°. The measured center frequency was 49.05 MHz, electromechanical coupling coefficient was 0.66, dielectric constant was 1178, and strain constant was 26.90 C/m^2, which all agreed well with the analytical calculations. These results will be helpful in design and fabrication of high-frequency micromachined ultrasound transducers.

Keywords

Electromechanical response, 1-3 piezoelectric composite, etching slope, micro-electromechanical systems

Introduction

Piezoelectric 1-3 composite materials have been widely used due to their superior properties including high electromechanical coupling coefficient and low acoustic impedance (Benjamin, 2001; Lee et al., 2012; Smith, 1990). In comparison with conventional composite transducer fabrication methods such as dice-and-fill, stacked plates, or lamination techniques, micromachined single-crystal piezoelectric 1-3 composite transducer technology recently has become a superior method to fabricate high-frequency ultrasonic transducers and arrays (Jiang et al., 2006 and 2008; Sun et al., 2010; Yuan et al., 2006). This is because it takes the advantage of high electromechanical coupling coefficients of single-crystal piezoelectrics and fine patterning features of photolithography and reactive ion etching (RIE). Similar to all other piezoelectric composite materials, the properties of micromachined single-crystal piezocomposites are highly dependent on constituent materials and the local arrangement of the different phases. In specific, the piezoelectric single-crystal polymer interface (etched side wall) may play an important role in the resulted electromechanical coupling in piezocomposites (Sottos et al., 1993). Moreover, in actual RIE or Deep RIE processing, the side wall slope of etched piezoelectric pillars can be varied from 70° to close to 90° which greatly affect the transducer performance. Therefore, understanding the effect of side wall slope of micropillars on properties of micromachined 1-3 composites will be important in developing high-performance micromachined composite transducers. In this article, on the basis of 1-3 composite thickness-mode oscillation model developed by Smith and Auld (1991), the etched slope effect on the electromechanical behavior of micromachined 1-3 piezocomposites was

[1]Department of Mechanical and Aerospace Engineering, North Carolina State University, Raleigh, NC, USA
[2]Suzhou Institute of Biomedical Engineering and Technology, Chinese Academy of Sciences, Suzhou, China

Corresponding author:
Xiaoning Jiang, Department of Mechanical and Aerospace Engineering, North Carolina State University, Raleigh, NC 27695, USA.
Email: xjiang5@ncsu.edu

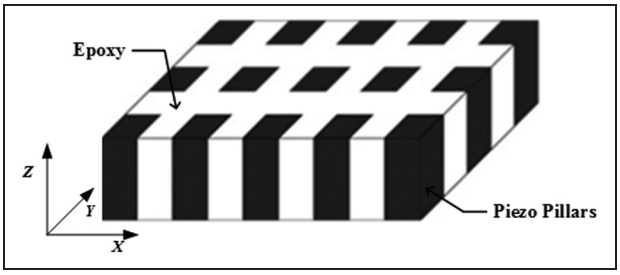

Figure 1. Schematic of a typical 1-3 piezocomposite structure.

investigated first by theoretical analysis, followed by finite element modeling and experimental verifications.

Structure of 1-3 piezocomposite with tapered pillars

A typical 1-3 piezocomposite structure is schematically shown in Figure 1. The black square pillars are piezoelectric materials, and the white part connecting all piezo pillars is epoxy. In conventional 1-3 piezocomposite structure fabricated by dice-and-fill technique, the side wall of pillars is usually vertical to their top and bottom surfaces. However, in micromachined 1-3 piezocomposite structures, side wall angle of etched piezo pillars is usually not 90° due to the redeposition process in etching of complex oxide (Jiang et al., 2006, 2008). Figure 2 shows the scanning electron microscope (SEM) pictures of etched single-crystal $(1-x)[Pb(Mg_{1/3}Nb_{2/3})O_3]$–$x[PbTiO_3]$ (PMN-PT) micropillars. One can observe that the side view of etched micropillars is not square any more, and the slope becomes more obvious when etching time is longer (Figure 2(b)).

Suggested by the above SEM pictures, pillars in the etched 1-3 piezocomposites were then approximately modeled as truncated pyramids, as shown in Figure 3.

According to the 1-3 composite thickness-mode oscillation model, the volume fraction is the key parameter which greatly decides the performance of composite (Smith and Auld, 1991). For example, the composite acoustic impedance, density, elastic stiffness, and piezoelectric constant increase essentially linearly with volume fraction, and furthermore, the electromechanical coupling constant and longitudinal velocity vary with the volume fraction too. To apply the model in this study, the volume fraction v of single-crystal piezoelectric material in the composite can then be expressed as

$$v = \frac{\frac{1}{3}[(r^2 + (r + 2h\text{ct}\, g\theta)^2 + r(r + 2h\text{ct}\, g\theta)]}{(r + d)^2} = \frac{r^2 + 2rh\text{ct}\, g\theta + 4h^2\text{ct}\, g^2\theta/3}{(r + d)^2} \quad (1)$$

where θ is the slope angle, r is the top surface side width of a PMN-PT pillar, d is the kerf width on top surface, and h is the height of PMN-PT pillar. For achieving high center frequency and good performance, r, d, and h are considered to be constants as designed (r = 15.9 μm, d = 5.1 μm, and h = 42.8 μm) referring to the reported works (Jiang et al., 2006, 2008; Yuan et al., 2006); the volume fraction of PMN-PT in the micromachined 1-3 composites will change with the etched slope angle θ, as shown in Figure 4. When the

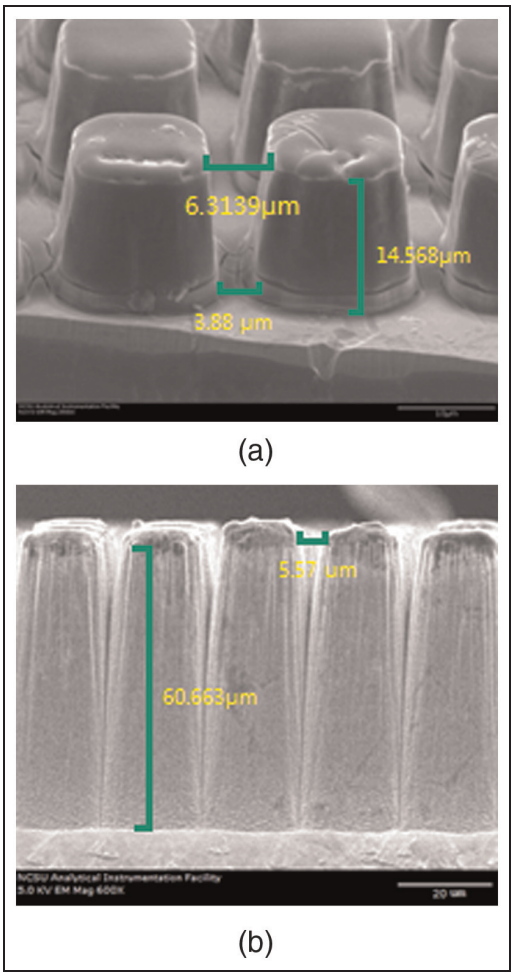

Figure 2. SEM pictures of etched PMN-PT pillars after (a) 30-min etching and (b) 3-h etching.
SEM: scanning electron microscope.

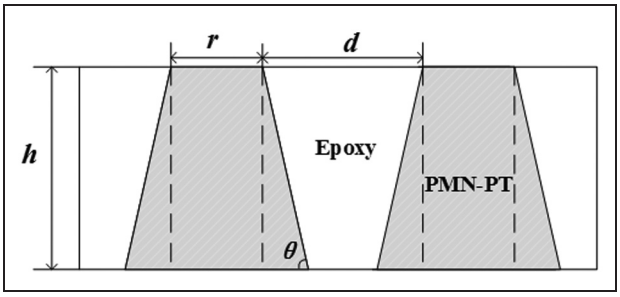

Figure 3. 1-3 composite structure with tapered pillars.
PMN-PT: $Pb(Mg_{1/3}Nb_{2/3})O_3$-$PbTiO_3$.

slope angle is 90°, the side wall will be perpendicular to the surface as designed, and the volume fraction will reach the minimum 57.3%. When the slope angle is 83.5°, the volume fraction will be about 100%. This is because in this case, the bottom of pillars would be overlapped in our model. In addition, if different parameter values of r, d, and h were used, a smaller slope minimum angle than 83.5° would be allowed.

Micromechanics of micromachined 1-3 piezocomposites

In conventional 1-3 piezocomposite structures, poling direction is usually along the z direction and the x–y plane as the isotropic electrode plane (Figure 1). Constitutive equations for piezo materials poled in the z direction can then be written in the matrix form (Standards Committee of the IEEE Ultrasonics, 1988)

$$\begin{Bmatrix} D_1 \\ D_2 \\ D_3 \end{Bmatrix} = \begin{bmatrix} 0 & 0 & 0 & 0 & d_{15} & 0 \\ 0 & 0 & 0 & d_{15} & 0 & 0 \\ d_{31} & d_{31} & d_{33} & 0 & 0 & 0 \end{bmatrix} \begin{Bmatrix} T_1 \\ T_2 \\ T_3 \\ T_4 \\ T_5 \\ T_6 \end{Bmatrix} + \begin{bmatrix} \varepsilon_{11}^T & 0 & 0 \\ 0 & \varepsilon_{11}^T & 0 \\ 0 & 0 & \varepsilon_{33}^T \end{bmatrix} \begin{Bmatrix} E_1 \\ E_2 \\ E_3 \end{Bmatrix} \quad (2)$$

$$\begin{Bmatrix} S_1 \\ S_2 \\ S_3 \\ S_4 \\ S_5 \\ S_6 \end{Bmatrix} = \begin{bmatrix} s_{11}^E & s_{12}^E & s_{13}^E & 0 & 0 & 0 \\ s_{12}^E & s_{11}^E & s_{13}^E & 0 & 0 & 0 \\ s_{13}^E & s_{13}^E & s_{33}^E & 0 & 0 & 0 \\ 0 & 0 & 0 & s_{44}^E & 0 & 0 \\ 0 & 0 & 0 & 0 & s_{44}^E & 0 \\ 0 & 0 & 0 & 0 & 0 & 2(s_{44}^E - s_{12}^E) \end{bmatrix} \begin{Bmatrix} T_1 \\ T_2 \\ T_3 \\ T_4 \\ T_5 \\ T_6 \end{Bmatrix} + \begin{bmatrix} 0 & 0 & d_{31} \\ 0 & 0 & d_{31} \\ 0 & 0 & d_{33} \\ 0 & d_{15} & 0 \\ d_{15} & 0 & 0 \\ 0 & 0 & 0 \end{bmatrix} \begin{Bmatrix} E_1 \\ E_2 \\ E_3 \end{Bmatrix} \quad (3)$$

where d_{ij} is the piezoelectric charge coefficient (i, j = 1, 2, 3, 4, 5, 6 stand for different directions x, y, z and their rotations (shear)), D_i is the dielectric displacement vector component, T_i is the stress component, ε_{ij} is the dielectric constant, E_i is the electric field vector component, S_i is the strain component, and s_{ij} is the elastic compliance coefficient. Because the epoxy phase is an isotropic homogeneous medium and piezoelectrically inactive, stress and electric displacement in epoxy phase can then be calculated as (Smith and Auld, 1991)

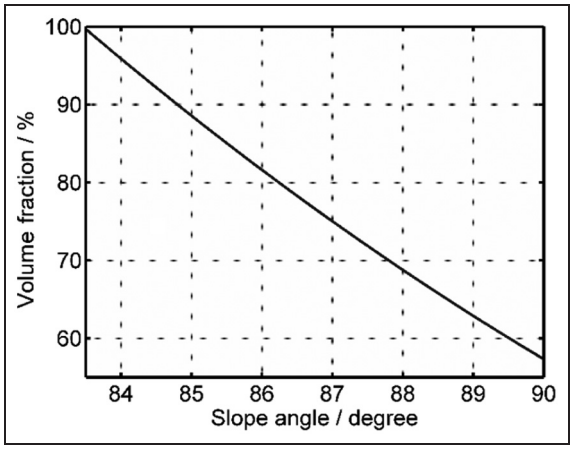

Figure 4. The volume fraction changes with the etched slope angle (r = 15.9 μm, d = 5.1 μm, and h = 42.8 μm).

$$\begin{aligned} T_1 &= c_{11}S_1 + c_{12}S_2 + c_{12}S_3 \\ T_2 &= c_{12}S_1 + c_{11}S_2 + c_{12}S_3 \\ T_3 &= c_{12}S_1 + c_{12}S_2 + c_{11}S_3 \\ T_4 &= c_{44}S_4 \\ T_5 &= c_{44}S_5 \\ T_6 &= c_{44}S_6 \\ D_1 &= \varepsilon_{11}E_1 \\ D_2 &= \varepsilon_{11}E_2 \\ D_3 &= \varepsilon_{11}E_3 \end{aligned} \quad (4)$$

where c_{ij} is the elastic stiffness coefficient. Pillar stress and electric displacement in PMN-PT phase can be expressed as (Smith and Auld, 1991)

$$\begin{aligned} T_1 &= c_{11}S_1 + c_{12}S_2 + c_{13}S_3 - e_{31}E_3 \\ T_2 &= c_{12}S_1 + c_{11}S_2 + c_{13}S_3 - e_{31}E_3 \\ T_3 &= c_{13}S_1 + c_{13}S_2 + c_{33}S_3 - e_{33}E_3 \\ T_4 &= c_{44}S_4 - e_{15}E_2 \\ T_5 &= c_{44}S_5 - e_{15}E_1 \\ T_6 &= c_{66}S_6 \\ D_1 &= e_{15}S_5 + \varepsilon_{11}E_1 \\ D_2 &= e_{15}S_4 + \varepsilon_{11}E_2 \\ D_3 &= e_{31}S_1 + e_{31}S_2 + e_{33}S_3 + \varepsilon_{33}E_3 \end{aligned} \quad (5)$$

where e_{ij} is the piezoelectric coefficient.

Then, according to Smith and Auld's 1-3 composite thickness-mode oscillation model, add the usual simplifications and approximations made in analyzing this thickness-mode oscillations in a large, thin, electroded piezo plate (symmetry in the x–y plane, $E_1 = E_2 = 0$, etc.). The final constitutive relations of effective total stress $\overline{T_3}$ and electric displacement $\overline{D_3}$ are

$$\begin{aligned} \overline{T_3} &= \bar{c}_{33}^E \bar{S}_3 - \bar{e}_{33}\bar{E}_3 \\ \overline{D_3} &= \bar{e}_{33}\bar{S}_3 + \bar{\varepsilon}_{33}^S \bar{E}_3 \end{aligned} \quad (6)$$

where $\bar{S}_3$ is the vertical strain of composite, $\bar{E}_3$ is the electric field of composite in z direction, details can be found in Smith and Auld (1991) and in our study, and $\bar{c}_{33}^E$, $\bar{e}_{33}$, and $\bar{\varepsilon}_{33}^S$ can be expressed as

$$\begin{aligned}
\bar{c}_{33}^E &= \frac{r^2 + 2rh\mathrm{ctg}\theta + 4h^2\mathrm{ctg}^2\theta/3}{(r+d)^2} \\
&\left[c_{33}^e - \frac{2(d^2 + 2rd - 2rh\mathrm{ctg}\theta - 4h^2\mathrm{ctg}^2\theta/3)(c_{13}^p - c_{12}^e)^2}{(r^2 + 2rh\mathrm{ctg}\,\theta + 4h^2\mathrm{ctg}^2\theta/3)(c_{11}^e + c_{12}^e) + (d^2 + 2rd - 2rh\mathrm{ctg}\,\theta - 4h^2\mathrm{ctg}^2\theta/3)(c_{11}^p + c_{12}^p)}\right] \\
&+ \frac{(d^2 + 2rd - 2rh\mathrm{ctg}\,\theta - 4h^2\mathrm{ctg}^2\theta/3)c_{11}^e}{(r+d)^2} \\
\bar{e}_{33} &= \frac{r^2 + 2rh\mathrm{ctg}\,\theta + 4h^2\mathrm{ctg}^2\theta/3}{(r+d)^2} \\
&\left[e_{33}^p - \frac{2(d^2 + 2rd - 2rh\mathrm{ctg}\,\theta - 4h^2\mathrm{ctg}^2\theta/3)e_{31}^p(c_{13}^p - c_{12}^e)}{(r^2 + 2rh\mathrm{ctg}\,\theta + 4h^2\mathrm{ctg}^2\theta/3)(c_{11}^e + c_{12}^e) + (d^2 + 2rd - 2rh\mathrm{ctg}\,\theta - 4h^2\mathrm{ctg}^2\theta/3)(c_{11}^p + c_{12}^p)}\right] \\
\bar{\varepsilon}_{33}^S &= \frac{r^2 + 2rh\mathrm{ctg}\theta + 4h^2\mathrm{ctg}^2\theta/3}{(r+d)^2} \\
&\left[\varepsilon_{33}^e - \frac{2(d^2 + 2rd - 2rh\mathrm{ctg}\,\theta - 4h^2\mathrm{ctg}^2\theta/3)(e_{31}^p)^2}{(r^2 + 2rh\mathrm{ctg}\,\theta + 4h^2\mathrm{ctg}^2\theta/3)(c_{11}^e + c_{12}^e) + (d^2 + 2rd - 2rh\mathrm{ctg}\,\theta - 4h^2\mathrm{ctg}^2\theta/3)(c_{11}^p + c_{12}^p)}\right] \\
&+ \frac{(d^2 + 2rd - 2rh\mathrm{ctg}\,\theta - 4h^2\mathrm{ctg}^2\theta/3)\varepsilon_{11}}{(r+d)^2}
\end{aligned} \tag{7}$$

By incorporating these effective material parameters into the thickness-mode oscillation analysis of a thin piezoelectric plate, one can obtain the electromechanical coupling coefficient K_t as

$$K_t = \frac{\bar{e}_{33}}{\sqrt{\bar{c}_{33}^E\bar{\varepsilon}_{33}^S + (\bar{e}_{33})^2}} \tag{8}$$

and the acoustic impedance Z of micromachined 1-3 composite can be calculated as

$$Z = \sqrt{\bar{c}_{33}^E\bar{\rho} + (\bar{e}_{33})^2\bar{\rho}/\bar{\varepsilon}_{33}^S} \tag{9}$$

where $\bar{\rho}$ is the composite density

$$\bar{\rho} = v\rho^p + (1-v)\rho^e \tag{10}$$

Results and discussions

With the above-mentioned model, a parametric study was carried out to assess the effect of the side wall angle of etched pillars on the properties of micromachined 1-3 piezocomposite. Material properties of piezoelectric single-crystal PMN-30%PT ($Pb(Mg_{1/3}Nb_{2/3})O_3$-$PbTiO_3$; HC Materials, Bolingbrook, IL, USA) and epoxy EPO-TEK 301 (Epoxy Technology Inc., Billerica, MA, USA) are presented in Table 1.

Composite mechanical and dielectric properties versus side wall angle

Substituting the material properties in Table 1 into equations (7) and (10), the mechanical properties of composites including density, elastic property, and the dielectric constant of the composite were obtained (Figure 5). For comparison with the experimental results, the parameters r, d, and h were set as the same parameters as those measured from the prototyped sample, in which r = 15.9 μm, d = 5.1 μm, and h = 42.8 μm. In Figure 5(a), the composite density ρ varies linearly with the etched slope angle when the length of r, d, and h is constant just as assumed above. In Figure 5(b), the strain constant e_{33} also varies almost linearly with the slope angle except around 83.5°. This is because according to equation (13), when the slope

Table 1. Key material properties of PMN-PT and EPO-TEK 301 (Jiang et al., 2003; Wang et al., 2001; Zhang et al., 2002).

PMN-PT			
ρ (kg/m^3)	8060	c_{11}^p (10^{10} N/m^2)	11.5
s_{11}^p (10^{-12} m^2/N)	52	c_{12}^p (10^{10} N/m^2)	10.5
s_{33}^E (10^{-12} m^2/N)	67.7	c_{13}^p (10^{10} N/m^2)	10.1
ε_{11}^s (μF/m)	29.1	c_{33}^p (10^{10} N/m^2)	10.8
ε_{33}^T (μF/m)	68.6	e_{31}^p (C/m^2)	−2.4
d_{33}^p (pC/N)	2900	e_{33}^p (C/m^2)	27.1
EPO-TEK 301			
ρ (kg/m^3)	1500	c_{11}^e (10^{10} N/m^2)	0.81
ε_{11}^e (pF/m)	33.63	c_{12}^e (10^{10} N/m^2)	0.81
s_{11}^e (10^{-12} m^2/N)	216	s_{12}^e (10^{-12} m^2/N)	−78

PMN-PT: $Pb(Mg_{1/3}Nb_{2/3})O_3$-$PbTiO_3$.

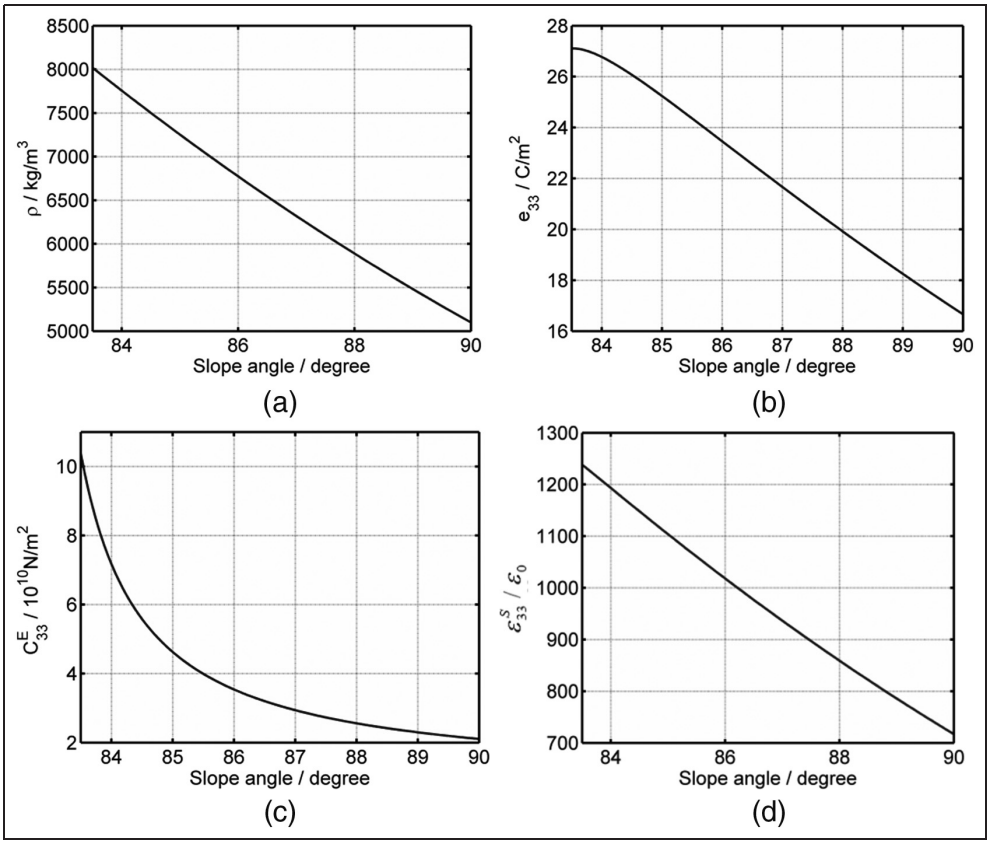

Figure 5. Dependence of composite properties on slope angle of pillars. (a) Variation in composite density ρ with slope angle. (b) Variation in strain constant e_{33} with slope angle. (c) Variation in stiffness c_{33}^E with slope angle. (d) Variation in dielectric constant $\varepsilon_{33}^S/\varepsilon_0$ with slope angle (r = 15.9 μm, d = 5.1 μm, and h = 42.8 μm).

angle is near 83.5°, the volume fraction of PMN-PT will almost reach 100%. In this situation, the e_{33} of composite will become the e_{33}^p of PMN-PT which is about 27.1 C/m^2 (Zhang et al., 2002). In Figure 5(c), the stiffness c_{33}^E will also decrease with the slope angle. Especially when the slope angle is smaller than 86°, the c_{33}^E will change rapidly. That can be explained as such that when the slope angle is smaller than 86°, the epoxy volume fraction will be very small, and hence, the epoxy contribution to the composite stiffness will be quite little. In Figure 5(d), $\varepsilon_{33}^s/\varepsilon_0$ also decreases linearly with the slope angle (ε_0 is the permittivity of vacuum (8.85×10^{-12} F/m)), which is similar to the variation in density ρ.

Electromechanical coupling coefficient and acoustic impedance of micromachined composites

The slope angle effect on electromechanical coupling coefficient K_t and acoustic impedance Z are shown in Figures 6 and 7, respectively. It was found that electromechanical coupling coefficient K_t increases with the slope angle. This is because in 1-3 piezocomposite, the surrounding epoxy causes the diminution of lateral clamping and makes more efficient power transfer to the thickness oscillation than in pure thickness mode, while the epoxy volume fraction decreased with the slope angle (Figure 4). But if the volume fraction of the epoxy is too much, the large amount of surrounding epoxy will stiffen the thin pillars and cause the decrease in K_t (Smith and Auld, 1991). While at the low end (slope angle round 83.5°), the composite almost becomes pure PMN-PT material, and the K_t is approached to the coupling coefficient 0.62 for a solid PMN-PT plate (Zhang et al., 2002). Therefore, for obtaining larger K_t, the etched side wall of PMN-PT should be made as vertical as possible.

The acoustic impedance Z increases rapidly as the slope angle decreases (Figure 7), especially at the low slope angle end where the merged pillar bottom brings up the piezo volume fraction as well as the acoustic impedance.

The variation in composite sound speed and frequency with slope angle

Sound speed and center frequency are essential for composite transducer design. Usually, the resonance frequency f can be expressed as

$$f = v_l/2h \tag{11}$$

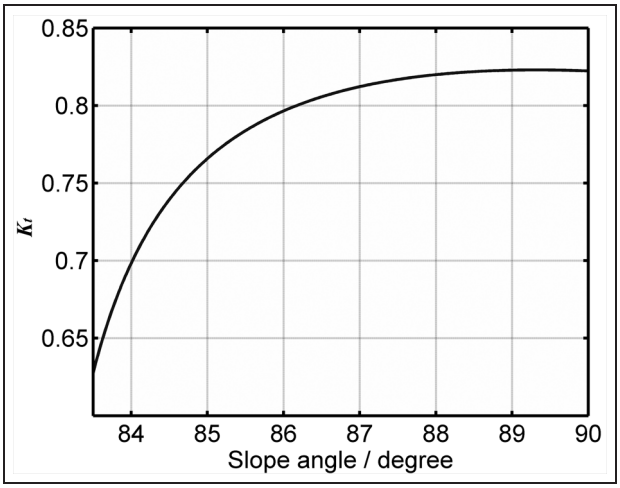

Figure 6. Variation in electromechanical coupling coefficient K_t with slope angle (r = 15.9 μm, d = 5.1 μm, and h = 42.8 μm).

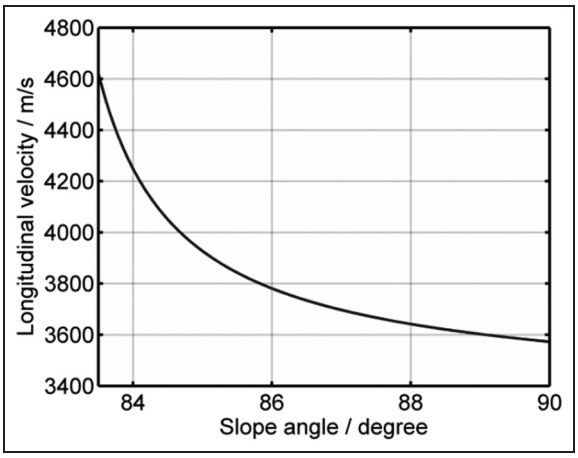

Figure 8. Variation in longitudinal velocity with slope angle (r = 15.9 μm, d = 5.1 μm, and h = 42.8 μm).

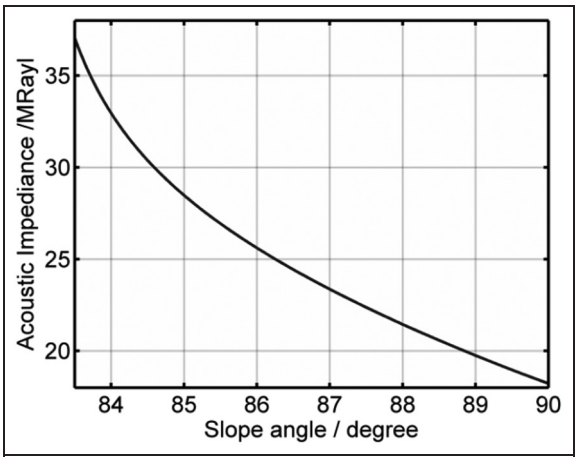

Figure 7. Variation in acoustic impedance with slope angle (r = 15.9 μm, d = 5.1 μm, and h = 42.8 μm).

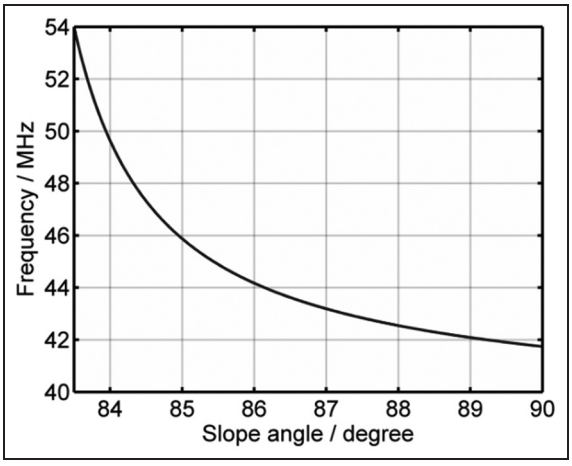

Figure 9. Variation in frequency with slope angle (r = 15.9 μm, d = 5.1 μm, and h = 42.8 μm).

where v_l is the longitudinal velocity, in 1-3 composite piezoelectric thickness oscillation model (Smith and Auld, 1991)

$$v_l = \sqrt{\bar{c}_{33}^D/\bar{\rho}} = \sqrt{(\bar{c}_{33}^E + \bar{e}_{33}{}^2/\bar{\varepsilon}_{33}^S)/\bar{\rho}} \qquad (12)$$

From equations (7) and (12), we can find that the longitudinal velocity also changes with the slope angle (Figure 8). The velocity sweeps down at high slope angles due to the epoxy loading. Meanwhile, the velocity approaches to the maximum 4600 m/s, the speed of solid PMN-PT plate, when the slope angle is below 83.5°.

Substituting equation (12) into equation (11), the resonant frequency of the composite can be calculated as

$$f = \sqrt{(\bar{c}_{33}^E + \bar{e}_{33}{}^2/\bar{\varepsilon}_{33}^S)/\bar{\rho}}/2h \qquad (13)$$

Figure 9 showed the relationship between the composite resonant frequency and slope angle of micropillars. According to equation (13), when h is constant, the frequency will decrease with the slope angle. Therefore, for obtaining the designed frequency, when the slope angle is large, the etched thickness should be deeper. And in engineering process, the slope angle is usually hard to control, so the thickness of composite will be a better choice to get the desired frequency through precise lapping (Jiang et al., 2008).

COMSOL simulation results

COMSOL program (COMSOL Inc., Burlington, MA, USA) was used to simulate the resonance of micromachined 1-3 composites for comparison with results obtained using the analytical model (Satyanarayana et al., 2012). As an example shown in Figure 10, the composite structure composes of PMN-PT pyramid

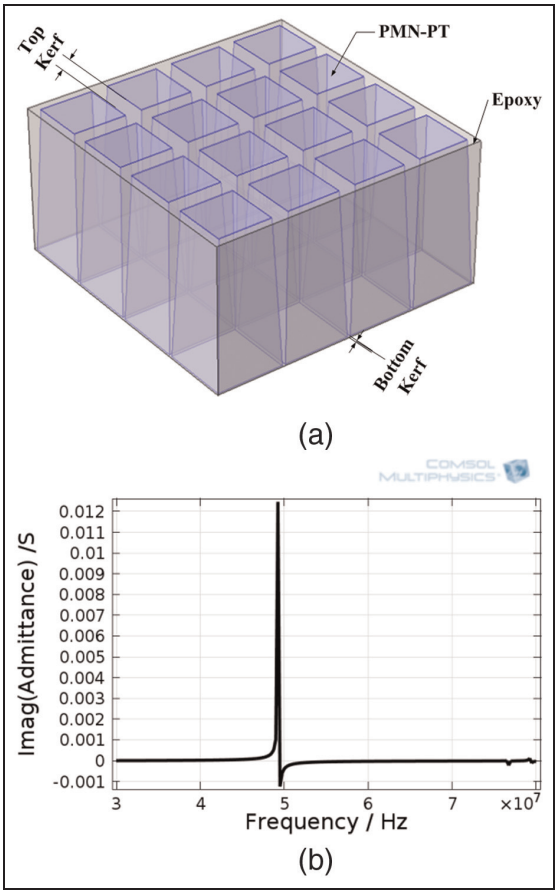

Figure 10. COMSOL simulation for composites with PMN-PT pyramid pillars and epoxy EPO-TEK 301. (a) COMSOL 1-3 composite model with slope angle and (b) the input susceptance as a function of excitation frequency ranged from 30 to 75 MHz. PMN-PT: $Pb(Mg_{1/3}Nb_{2/3})O_3$-$PbTiO_3$.

pillars and epoxy EPO-TEK 301. The pillar's top surface side length was 15.9 μm, bottom surface side length was 20 μm, the top surface kerf width was 5.1 μm, and the composite thickness was 42.8 μm. The corresponded side wall angle was 83.8°. The material properties are shown in Table 1. The COMSOL composite piezoelectric transducer module was chosen to build the simulation. The final susceptance (imaginary part of transducer admittance) curve was obtained as shown in Figure 10(b), and the peak was found at around 49.5 MHz, which is close to the frequency values calculated by the above-mentioned analytical model (Figure 9). For the slope angle of 90°, the susceptance curve obtained was as shown in Figure 11, in which the composite center frequency decreases to 42.5 MHz. This change in trend is satisfied with the theoretical expectations (Figure 9).

Experimental results

In order to validate the above-mentioned models, micromachined PMN-PT 1-3 piezoelectric composite

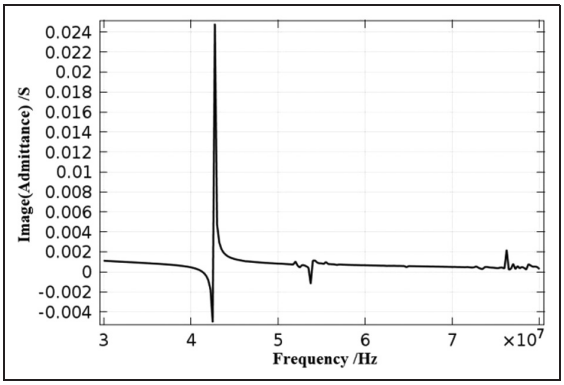

Figure 11. The input susceptance as a function of excitation frequency for composites with 90° side wall when r = 15.9 μm, d = 5.1 μm, and h = 42.8 μm.

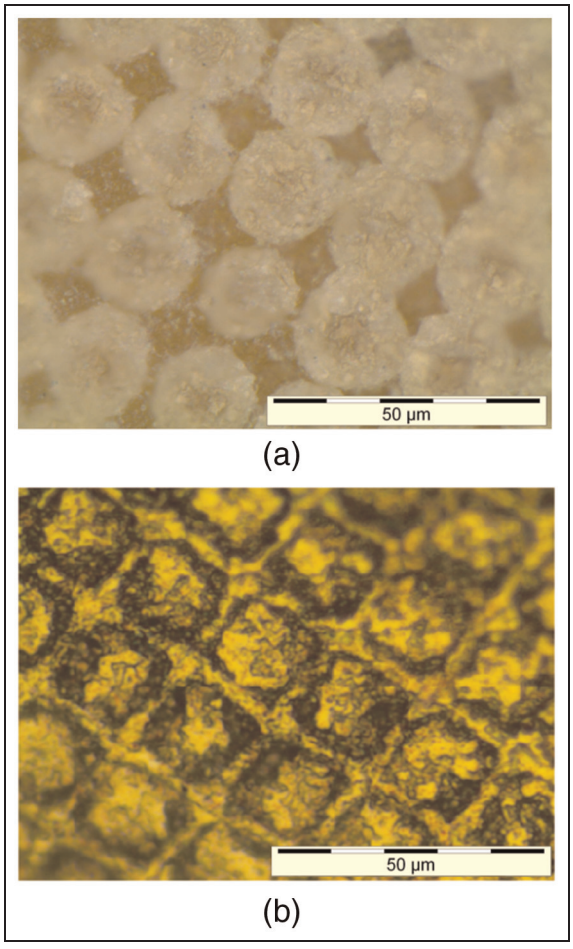

Figure 12. Photographs of PC-MUT composites: (a) bottom surface before electroplated and (a) top surface.
PC-MUT: piezoelectric composite–based micromachined ultrasound transducer.

sample was prepared (Figure 12), following the processes reported in Yuan et al. (2006). Because of the RIE effect, the corners of pillars were almost round, which was especially obvious in the bottom surface after lapping.

Table 2. Key material parameters of micromachined PMN-PT 1-3 piezoelectric composite sample.

Pillar material	PMN-30%PT	Epoxy	EPO-TEK 301
Size (mm × mm)	1.60 × 1.62	Thickness (μm)	42.80
Average pillar size of top surface (μm × μm)	15.90 × 15.90	Average kerf width of top surface (μm)	5.10
Average pillar size of bottom surface (μm × μm)	19.80 × 20.10	Average kerf width of bottom surface (μm)	0.95
Average slope angle (°)	83.80		

PMN-PT: $Pb(Mg_{1/3}Nb_{2/3})O_3$-$PbTiO_3$.

Table 2 summarizes the key measured parameters of the composite sample.

The electrical impedance spectrum, as shown in Figure 13, was measured using an impedance analyzer (4294A; Agilent Technologies, Englewood, CO, USA). It was found that the center frequency of the prepared 1-3 composite is about 49 MHz, which agrees well with the results calculated from the analytical model and COMSOL model (see Figures 9 and 10).

With the measured impedance spectrum, the electromechanical coupling coefficient K_t can also be calculated as (Safari and Akdoğan, 2008)

$$K_t = \sqrt{\frac{\pi}{2} \times \frac{f_s}{f_p} \times \mathrm{tg}\left(\frac{\pi}{2} \times \frac{f_p - f_s}{f_p}\right)} \tag{14}$$

where f_s is the resonant frequency at which the conductance reaches the minimum and f_p is the parallel resonant frequency at which the resistance reaches the maximum. In our sample, the f_s was 42 MHz, and the f_p was 54 MHz, so the calculated K_t was about 0.66, which was close to the calculated value 0.67 (Figure 6).

Besides the electromechanical coupling coefficient, we also measured the capacitance of the prototyped sample, which was 643.28 pF. Then, according to the capacitance calculation equation (Standards Committee of the IEEE Ultrasonics, 1988)

$$C = \varepsilon_r \varepsilon_0 \frac{A}{d} = \bar{\varepsilon}_{33}^{s} \frac{A}{d} \tag{15}$$

where A is the area of electrode surfaces and d is the separation between the plates (the thickness). The dielectric constant $\bar{\varepsilon}_{33}^{S}$ was obtained as 1178.4, which is similar to the calculated value (1200) from the above-mentioned model with slope angle of 83.8°. (Figure 5(d)).

Furthermore, the sample stiffness was also calculated according to flow formula (Kwok et al., 1997; Standards Committee of the IEEE Ultrasonics, 1988)

$$\begin{aligned} c_{33}^{D} &= 4\bar{\rho}h^2 f_p^2 \\ c_{33}^{E} &= c_{33}^{D}(1 - K_t^2) \end{aligned} \tag{16}$$

Substituting the above-mentioned related parameter values into equation (16), the c_{33}^{E} was calculated to be 8.94×10^{10} N/m^2. It is a little bigger than the calculated result (8.17×10^{10} N/m^2) from the above-mentioned model (Figure 5(c)); this is because according to above-mentioned analytical model around slope angle 83.8°, the stiffness will sharply change, and the detected slope angle may have a small tolerance caused by the anisotropy of etching.

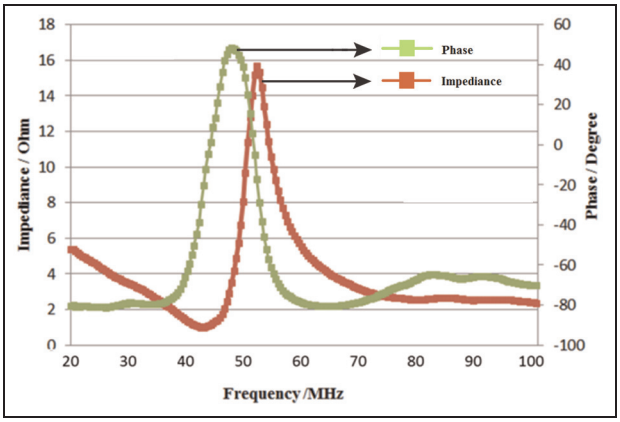

Figure 13. Impedance and phase versus frequency of a 42.8-μm-thick PMN-PT/epoxy 1-3 composite sample.
PMN-PT: $Pb(Mg_{1/3}Nb_{2/3})O_3$-$PbTiO_3$.

The strain constant e_{33} was then obtained using the flow relationship (Kwok et al., 1997)

$$e_{33} = K_t \sqrt{\varepsilon_{33}^{s} c_{33}^{D}} \tag{17}$$

The calculated e_{33} was 26.90 C/m^2, which also agrees well with the model's expected value of 26.86 C/m^2 (Figure 5(b)).

Finally, all the referenced parameters of the micromachined 1-3 piezocomposite including analytical model results and experimental measurements were summarized and listed in Table 3.

Conclusion

A modified thickness-mode oscillation model was developed to investigate the effect of side wall angle of etched micropillars on electromechanical characteristics of micromachined 1-3 piezoelectric composites. With this analytical model, the composite properties including strain constant, stiffness, dielectric constant, electromechanical coupling coefficient, acoustic impedance, longitudinal velocity, and frequency can be calculated. The calculation results showed that the electromechanical coupling coefficient K_t increases with the slope

Table 3. Key material parameter comparison of micromachined PMN-PT 1-3 piezoelectric composite sample between model calculated results and experimental measurements.

	$\bar{\rho}$ (kg/m^3)	$\bar{e}_{33}$ (C/m^2)	$\bar{c}^E_{33}$ (10^{10} N/m^2)	$\bar{\varepsilon}_{33}$ (ε_0)	f (MHz)	K_t
Model	7812	26.86	8.17	1200	50.15	0.67
Experiment	7750	26.90	8.94	1178	49.05	0.66

PMN-PT: $Pb(Mg_{1/3}Nb_{2/3})O_3$-$PbTiO_3$.

angle, while the acoustic impedance and center frequency decrease with side wall angle. The measured resonant frequency was 49.05 MHz for the fabricated 1-3 composite with 15.9 μm side length pillar, 5.1 μm top surface kerf, 0.95 μm bottom surface kerf, 42.8 μm thickness, and 83.8° slope angle, which agrees well with the results from the analytical model and the COMSOL simulation. The measured electromechanical coupling coefficient was 0.66, which is also close to the calculated result. Although because of the RIE effect, the slope angle will vary in a small range, when the average slope angle was used, the deviation of our analytical model and experiment is smaller than 5% which is acceptable; the detailed comparison can be found in Table 3. These results provide a rich set of options for the piezoelectric transducer design and fabrication by considering the effect of etched slope and hence are important for developing high-performance high-frequency composite transducers for both medical imaging and industrial nondestructive testing applications.

Acknowledgement

We thank our anonymous reviewers for their feedback and support which greatly improved the content of this article.

Declaration of conflicting interests

The authors declared no potential conflicts of interest with respect to the research, authorship, and/or publication of this article.

Funding

This work was supported by the National Key Technology Research and Development Program of the Ministry of Science and Technology of China (grant no. 2012BAI13B02), National Natural Science Funds for Young Scholar of China (grant no. 11204198), the Funds for Technology of Suzhou, China (grant no. SYG201433).

References

Benjamin KC (2001) Recent advances in 1-3 piezoelectric polymer composite transducer technology for AUV/UUV acoustic imaging applications. In: *MTS/IEEE conference and exhibition OCEANS*, Honolulu, HI, 5–8 November, pp. 26–33. New York: IEEE.

Lee JH, Zhang S, Geng X, et al. (2012) Electroacoustic response of 1-3 piezocomposite transducers for high power applications. *Applied Physics Letters* 101: 253504.

Jiang W, Zhang R, Jiang B, et al. (2003) Characterization of piezoelectric materials with large piezoelectric and electromechanical coupling coefficients. *Ultrasonics* 41: 55–63.

Jiang X, Yuan J, Cheng A et al. (2006) Microfabrication of piezoelectric composite ultrasound transducers (PC-MUT). In: IEEE Ultrasonics Symposium, Vancouver,BC, Canada, 3-6 October, pp. 918-921. New York: IEEE.

Jiang X, Snook K, Cheng A, et al. (2008) Micromachined PMN-PT single crystal composite transducers—15–75 MHz PC-MUT. In: *2008 IEEE ultrasonics symposium*, Beijing, China, *2–5 November*, pp. 164–167. New York: IEEE.

Kwok KW, Chan HLW and Choy CL. (1997) Evaluation of the material parameters of piezoelectric materials by various methods. *IEEE Transactions on Ultrasonics, Ferroelectrics and Frequency Control* 44: 733–742.

Safari A and Akdoğan EK (2008) *Piezoelectric and Acoustic Materials for Transducer Applications*. New York: Springer.

Satyanarayana T, Srinivas G, Prasad MS, et al. (2012) Design and analysis of MEMS based composite piezoelectric ultrasonic transducer. *Electrical and Electronic Engineering* 2: 362–373.

Smith WA (1990) The application of 1-3 piezocomposites in acoustic transducers. In: *IEEE 7th international symposium on applications of ferroelectrics*, Urbana-Champaign, IL, 6–8 June, pp. 145–152. New York: IEEE.

Smith WA and Auld BA (1991) Modeling 1-3 composite piezoelectrics: thickness-mode oscillations. *IEEE Transactions on Ultrasonics, Ferroelectrics and Frequency Control*38: 40–47.

Sottos NR, Li L, Scott WR, et al. (1993) Micromechanical behavior of 1-3 piezocomposites. In: *Proceedings of SPIE 1916, smart structures and materials 1993: smart materials*, Albuquerque, NM, 1 February, pp. 87–96. Bellingham, WA: SPIE.

Standards Committee of the IEEE Ultrasonics (1988) IEEE Standard on Piezoelectricity. ANSI/IEEE Std 176–1987: 0–1. Available at: http://ieeexplore.ieee.org/xpl/mostRecentIssue.jsp?punumber=2511

Sun P, Wang G, Wu D, et al. (2010) High frequency PMN-PT 1-3 composite transducer for ultrasonic imaging application. *Ferroelectrics* 408: 120–128.

Wang H, Ritter T, Cao W, et al. (2001) High frequency properties of passive materials for ultrasonic transducers. *IEEE Transactions on Ultrasonics, Ferroelectrics and Frequency Control* 48: 78–84.

Yuan J, Jiang X, Snook K, et al. (2006) 5I-1 Microfabrication of piezoelectric composite ultrasound transducers (PC-MUT). In: *IEEE ultrasonics symposium*, Vancouver, BC, Canada, 2–6 October, pp. 922–925. New York: IEEE.

Zhang R, Jiang W, Jiang B, et al. (2002) Elastic, dielectric and piezoelectric coefficients of domain engineered 0.70 Pb (MgNb) O-0.30 PbTiO single crystal. *AIP conference proceedings* 626: 188–197.